Geometry of large-scale low-energy excitations in the one-dimensional Ising spin glass with power-law interactions

Helmut G. Katzgraber[1] and A. P. Young[2,*]
[1]*Theoretische Physik, ETH Hönggerberg, CH-8093 Zürich, Switzerland*
[2]*Department of Physics, University of California, Santa Cruz, California 95064, USA*
(Received 23 July 2003; published 8 December 2003)

Results are presented for the geometry of low-energy excitations in the one-dimensional Ising spin chain with power-law interactions, in which the model parameters are chosen to yield a finite spin-glass transition temperature. Both finite-temperature and ground-state studies are carried out. For the range of sizes studied the data cannot be fitted to any of the standard spin-glass scenarios without including corrections to scaling. Incorporating such corrections we find that the fractal dimension of the surface of the excitations, is either equal to the space dimension, consistent with replica symmetry breaking, or very slightly less than it. The latter case is consistent with the droplet and ''trivial-nontrivial'' pictures.

DOI: 10.1103/PhysRevB.68.224408 PACS number(s): 75.50.Lk, 75.40.Mg, 05.50.+q

I. INTRODUCTION

There have been several numerical attempts at finite temperature[1–8] and zero temperature[9–16] to better understand the nature of the spin-glass state for short-range spin glasses. These results are generally interpreted in terms of the two main theories for the spin-glass phase: the replica symmetry-breaking (RSB) picture,[17–20] and the ''droplet picture''[21–24] (DP). RSB predicts that excitations involving a finite fraction of the spins cost only a finite energy in the thermodynamic limit, and that the fractal dimension of the *surface* of these excitations d_s is equal to the space dimension d. This is in contrast to DP where a low-energy excitation (droplet) has an energy proportional to ℓ^θ, where ℓ is the characteristic length scale of the droplet and θ is a positive stiffness exponent. In addition, the surface of these excitations is fractal with $d_s<d$. More recently Krzakala and Martin,[1] as well as Palassini and Young,[2] suggest an intermediate picture (called ''TNT'' for trivial-nontrivial) in which droplets have a fractal surface with $d_s<d$, and their energy is finite in the thermodynamic limit. Which of the above pictures describes the spin-glass state correctly is still widely debated.

The RSB and TNT pictures require two stiffness exponents for the energy of large-scale excitations. There is convincing numerical evidence that changing the boundary conditions (e.g., from periodic to antiperiodic), which induces a *domain wall*, costs an energy which increases as ℓ^θ with $\theta>0$. On the other hand, in the RSB and TNT pictures, the energy of *droplets*, created by thermal noise or by applying a perturbation for a fixed set of boundary conditions, varies as $\ell^{\theta'}$ with $\theta'=0$. By contrast, the DP makes the reasonable ansatz that $\theta'=\theta$ (>0).

In a previous publication,[25] we studied the one-dimensional long-range Ising spin glass with power-law interactions. The model's advantage is that large system sizes can be studied, in contrast to the short-range spin-glass models commonly used. The results of Ref. 25 showed that the stiffness exponent θ for zero-temperature domain-wall excitations is positive and in fair agreement with analytical predictions from the droplet model.[23,25,26] However, the stiffness exponent θ' for thermally induced droplet excitations is different and consistent with zero. Hence, *at least for the range of system sizes studied*, $L\leqslant 512$, the data of Ref. 25 are consistent with both the TNT and RSB scenarios since they have $\theta>\theta'=0$.

The purpose of the present paper is to estimate d_s, because this distinguishes between the RSB and TNT scenarios, since $d_s=d$ in RSB while $d_s<d$ in TNT. For short-range models, a droplet excitation forms a single connected piece, and so d_s has to be zero in $d=1$. However, for long-range interactions, a droplet may consist of disconnected pieces,[23] so a nontrivial value of d_s is possible in $d=1$. We perform both finite-temperature Monte Carlo simulations and ground-state studies. Our results suggest that droplets are possibly compact in agreement with RSB, although the data are also consistent with a very small value of $d-d_s$, which would be consistent with TNT.

In Sec. II we introduce the model, observables, and details of the Monte Carlo technique. Results at zero temperature are presented in Sec. III, and those at finite temperature are presented in Sec. IV. Our conclusions are summarized in Sec. V.

II. MODEL AND NUMERICAL METHOD

The Hamiltonian of the one-dimensional long-range Ising spin chain with power-law interactions is given by

$$\mathcal{H}=-\sum_{\langle i,j\rangle} J_{ij}S_iS_j, \tag{1}$$

where the Ising spins $S_i=\pm 1$ are evenly distributed on a circular ring of length L to ensure periodic boundary conditions. The sum is over all pairs of spins on the chain and the couplings J_{ij} are given by

$$J_{ij} = c(\sigma)\frac{\epsilon_{ij}}{r_{ij}^{\sigma}}, \tag{2}$$

where[25]

$$r_{ij} = \frac{L}{\pi}\sin\left(\frac{\pi|i-j|}{L}\right) \tag{3}$$

is the straight-line distance between sites i and j. The random part of the interactions ϵ_{ij} is chosen according to a Gaussian distribution with zero mean and standard deviation unity, and the constant $c(\sigma)$ in Eq. (2) is chosen[25] to give a mean-field transition temperature $T_c^{\mathrm{MF}}=1$.

The one-dimensional long-range Ising spin chain has a very rich phase diagram[23,26,25] in the d-σ plane. Spin-glass behavior is controlled by the long-range part of the interaction if σ is sufficiently small, and by the short-range part if σ is sufficiently large. In this work we focus on the long-range behavior at $\sigma=0.75$ for which[25] $T_c>0$ and the critical exponents are non-mean-field like. Using the exact relation[23,26] $\theta=d-\sigma$, we expect $\theta=0.25$ for $d=1$, which is in moderate agreement with numerical results[25] for *domain walls* induced by a change in boundary conditions at $T=0$. By studying thermally induced *droplet* excitations, Ref. 25 also estimated $\theta'\approx 0$, consistent with RSB and TNT.

In order to excite droplets at zero temperature we use the coupling-dependent ground-state perturbation method described elsewhere.[2,30,31] First, we compute the ground-state configuration $\{S_i^{(0)}\}$. Then we perturb the couplings J_{ij} by the following amount:

$$\Delta\mathcal{H}(\epsilon) = \frac{2\epsilon}{N}\sum_{\langle i,j\rangle}\frac{[J_{ij}^2]_{\mathrm{av}}}{(T_c^{MF})^2}S_i^{(0)}S_j^{(0)}S_iS_j, \tag{4}$$

where ϵ is a coupling constant and $[\cdots]_{\mathrm{av}}$ represents a disorder average. The (total) energy of the unperturbed ground state then increases by exactly ϵ, whereas the energy of any other state α will increase by the lesser amount of ϵq_l, where q_l is the link overlap between the unperturbed ground state and a state α:

$$q_l = \frac{2}{N}\sum_{\langle i,j\rangle}\frac{[J_{ij}^2]_{\mathrm{av}}}{(T_c^{MF})^2}S_i^{(\alpha)}S_j^{(\alpha)}S_i^{(0)}S_j^{(0)}. \tag{5}$$

In previous work q_l has been defined for nearest-neighbor models in which the sum is over nearest-neighbor pairs. Here we have generalized the link overlap to long-range models in a natural way. Because the coupling constant ϵ is of order unity and not of order L only low-energy excitations can be generated. We compute the new ground state of the perturbed system and record the link overlap between the old and new ground states. In the context of zero-temperature simulations the term ''link overlap'' will hereafter refer to the link overlap between the perturbed and unperturbed ground states.

Ground states are calculated using the parallel tempering Monte Carlo method[27,28] (at very low temperatures) as described in Refs. 25 and 32. The parameters used in the $T=0$ simulations are shown in Table I. For each value of L and ϵ we compute 10^4 disorder realizations. We find that for $\sigma=0.75$, when the model is in the long-range phase, the efficiency of the used algorithm to calculate ground states scales as L^z with $z=2.9\pm0.3$. For the current project this translates to a total CPU time of 70 CPU years on an Intel Pentium IV 2.4 GHz processor. Curiously, for $\sigma=2.50$, for which the interactions are effectively short range so frustration is minimal in the $d=1$ model studied here, the algorithm performs poorly with the equilibration time varying as $\sim\exp(aL)$, with $a=0.13\pm0.02$. It would be useful to understand intuitively the reasons for this.

TABLE I. Parameters of the $T=0$ simulations. The table shows the total number of Monte Carlo steps used for each value of ϵ and L. All data are computed with 10^4 disorder realizations. The lowest temperature used to calculate the ground states with parallel tempering Monte Carlo is $T=0.05$, the highest 1.70. We use between 10 and 23 temperatures, depending on the system size, to ensure that the acceptance ratios of the parallel tempering moves are larger than ~ 0.30.

ϵ	$L=16$	$L=32$	$L=64$	$L=128$	$L=256$	$L=512$
0.50	2×10^3	4×10^3	8×10^3	4.0×10^4	3.2×10^5	4.0×10^5
1.00	2×10^3	4×10^3	8×10^3	4.0×10^4	3.2×10^5	4.0×10^5
2.00	2×10^3	4×10^3	8×10^3	4.0×10^4	3.2×10^5	4.0×10^5

One quantity that we study at $T=0$ is the link overlap, averaged over *all samples*. To see how this varies with size[2] consider a large cluster of excited spins. This has a characteristic energy of order $\sim L^{\theta'}$, which is to be compared with the energy gained from the perturbation $\epsilon(1-q_l)\sim\epsilon L^{-(d-d_s)}$. There is a distribution of cluster energies which we assume to have a finite weight at the origin, so the probability that the perturbation will create the excitation is $\sim\epsilon L^{-(\theta'+d-d_s)}$. When this occurs $1-q_l\sim L^{-(d-d_s)}$, and so on average[2,30,31]

$$[1-q_l]_{\mathrm{av}} = \epsilon L^{-\mu_l}(a+bL^{-c}), \tag{6}$$

where

$$\mu_l = \theta' + 2(d-d_s) \tag{7}$$

and we have added a correction to scaling term bL^{-c}.

In RSB we have $\mu_l=0$ so Eq. (6) tends to a constant for $L\to\infty$, whereas in DP and TNT $\mu_l>0$ so Eq. (6) tends to zero in this limit.

TABLE II. Parameters of the finite-T simulations. N_{samp} is the number of samples, N_{sweep} is the total number of Monte Carlo sweeps for each of the $2N_T$ replicas for a single sample, and N_T is the number of temperatures used in the parallel tempering method.

L	N_{samp}	N_{sweep}	N_T
16	2.0×10^4	2.0×10^3	10
32	2.0×10^4	4.0×10^3	10
64	2.0×10^4	8.0×10^3	12
128	2.0×10^4	4.0×10^4	14
256	1.0×10^4	2.0×10^5	17
512	5.0×10^3	8.0×10^5	24

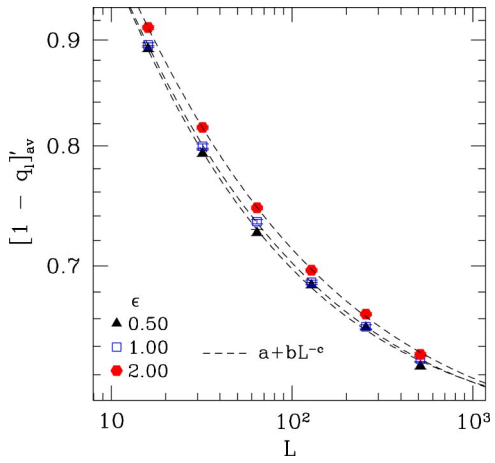

FIG. 1. Zero-temperature data for $[1-q_l]'_{\rm av}$ as a function of system size L for different values of the coupling constant ϵ. Note that the data only depend slightly on ϵ, thus indicating only small deviations from the scaling form. The dashed lines correspond to a three-parameter fit to $a+bL^{-c}$ as expected in RSB.

In addition, we consider averages over *only those samples in which a large excitation is generated*,[31,30] comprising a finite fraction of spins. The criterion we take is $|q|\leqslant 0.50$. Averaging just over these samples gives[31,30]

$$[1-q_l]'_{\rm av}=L^{-(d-d_s)}(a+bL^{-c}), \tag{8}$$

the prime representing the restricted average. Equation (8) follows trivially from the arguments presented in the derivation of Eq. (6) with the probability factor $\epsilon L^{-(\theta'+d-d_s)}$ replaced by unity. We expect that $[1-q_l]'_{\rm av}$ will be independent of ϵ.

In order to study droplet geometries at finite temperatures, we compute the distribution of the link overlap q_l between two replicas α and β of the system with the same disorder:

$$q_l=\frac{2}{N}\sum_{\langle i,j\rangle}\frac{[J_{ij}^2]_{\rm av}}{(T_c^{MF})^2}[\langle S_i^{(\alpha)}S_j^{(\alpha)}S_i^{(\beta)}S_j^{(\beta)}\rangle]_{\rm av}. \tag{9}$$

Here $\langle\cdots\rangle$ represents a thermal average, and $[\cdots]_{\rm av}$ represents a disorder average. From the finite-size scaling arguments[4] used to derive Eq. (6) we expect that the variance of the distribution of the link overlap scales as

$$\mathrm{Var}(q_l)=L^{-\mu_l}(a+bL^{-c}). \tag{10}$$

TABLE III. Fits of zero-temperature data for $[1-q_l]'_{\rm av}$ to $L^{-(d-d_s)}(a+bL^{-c})$, appropriate for DP/TNT, for different coupling constants ϵ. The last column is χ^2 per degree of freedom, where, for this data with six points and four fitting parameters, the number of degrees of freedom (ndf) is two.

ϵ	$d-d_s$	a	b	c	χ^2/ndf
0.50	0.043(14)	0.81(8)	1.95(64)	0.83(19)	0.64
1.00	0.003(28)	0.59(14)	1.29(7)	0.51(9)	0.31
2.00	0.019(19)	0.67(10)	1.30(8)	0.54(8)	1.63

TABLE IV. Fits of zero-temperature data for $[1-q_l]'_{\rm av}=a+bL^{-c}$, appropriate for RSB, for different values of the coupling constant ϵ. The number of degrees of freedom (ndf) here is three.

ϵ	a	b	c	χ^2/ndf
0.50	0.580(7)	1.35(8)	0.53(3)	1.74
1.00	0.575(6)	1.29(5)	0.50(2)	0.21
2.00	0.569(5)	1.28(4)	0.474(14)	1.36

Note that in RSB $\mu_l=0$ so $\mathrm{Var}(q_l)$ tends to a constant for $L\to\infty$. However, $\mu_l>0$ in DP (since $\theta'=\theta>0$ and $d_s<d$) and in TNT (since $d_s<d$). The bL^{-c} term is a correction to scaling, which turns out to be necessary since the data cannot be fitted without it.

To speed up equilibration of the finite-T simulations we use the parallel tempering Monte Carlo method.[27,28] We test for equilibration using the criterion developed earlier,[4] now generalized[25] for the Hamiltonian in Eq. (1). For all sizes, the lowest temperature used is $T=0.05$, well below $T_c\simeq 0.63$.[25,29] The highest temperature is 1.70 which is well above the mean-field critical temperature ($T_c^{\rm MF}=1$) and so the spins equilibrate fast there. We choose the spacing between the temperatures such that the acceptance ratios for the global moves are around 0.30. Parameters of the finite-T simulations are summarized in Table II.

To summarize, for $L\to\infty$ all the quantities that we calculate, $[1-q_l]_{\rm av}$ in Eq. (6), $[1-q_l]'_{\rm av}$ in Eq. (8), and $\mathrm{Var}(q_l)$ in Eq. (10) tend to a non-zero constant in RSB, whereas they tend to zero with a power of L in TNT and DP.

III. RESULTS AT ZERO TEMPERATURE

We first discuss the results for the constrained average of $1-q_l$, including only samples $|q|\leqslant 0.5$, since this yields $d-d_s$ independent of θ', see Eq. (8). The results are shown in Fig. 1. Note that the data only depend slightly on ϵ, indicating only small deviations from the expected scaling form.

The results of a DP/TNT fit to $[1-q_l]'_{\rm av}=L^{-(d-d_s)}(a$

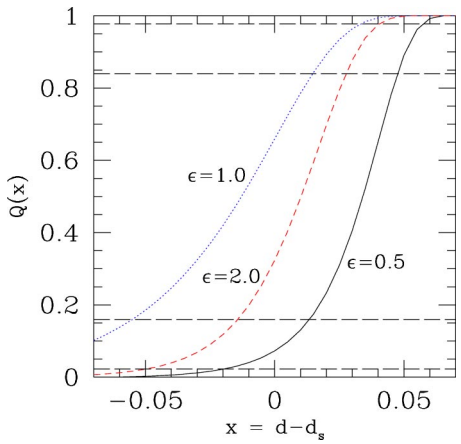

FIG. 2. The cumulative probability for $d-d_s$ from the fits to $[1-q_l]'_{\rm av}$ as discussed in the text. The inner pair of dashed horizontal lines show 68% confidence levels and the outer pair show 95.5% confidence levels.

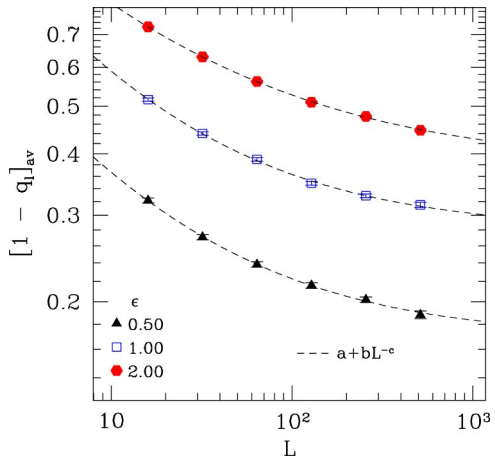

FIG. 3. Zero-temperature data for $[1-q_l]_{\rm av}$ as a function of system size L for different values of the coupling constant ϵ. The dashed lines represent fits according to $[1-q_l]_{\rm av}=a+bL^{-c}$ (RSB).

$+bL^{-c}$) are presented in Table III, while the corresponding RSB fits to $[1-q_l]'_{\rm av}=a+bL^{-c}$ are shown in Table IV. In the DP/TNT fits we find that $d-d_s$ is close to zero.

Both DP/TNT and RSB fits are acceptable ($\chi^2/{\rm ndf}\simeq 1$). However, in fits to a nonlinear model, one cannot convert $\chi^2/{\rm ndf}$ to a confidence limit[33] even if the data have a normal distribution. Similarly, unlike for the case for fits to a linear model, the error bars do not correspond to a 68% confidence. We are particularly interested to get a confidence limit on the value of $d-d_s$ in the DP/TNT fits. We do this by computing χ^2 as a function of $d-d_s$, minimizing with respect to the other parameters (a, b, and c). The probability of the fit P is proportional to $\exp(-\chi^2/2)$ which we numerically integrate to get the cumulative probability for $x=d-d_s$:

$$Q(x)=\int^x P(x')dx'. \tag{11}$$

The results are shown in Fig. 2. The data for $\epsilon=0.5$ and 2.0 constrain $d-d_s$ to zero or a small positive value. The data for $\epsilon=1.0$ constrain $d-d_s$ less and allow a range of negative values which are unphysical. At a 68% confidence level the data are consistent with

$$0\leqslant d-d_s\lesssim 0.05, \tag{12}$$

apart from the $\epsilon=0.5$ data which would exclude zero at the 68% level but, from Fig. 2, are consistent with it at the 86%

TABLE V. Fits of the zero-temperature data for $[1-q_l]_{\rm av}=L^{-\mu_l}(a+bL^{-c})$, which assume the DP/TNT picture, for different coupling constants ϵ.

ϵ	μ_l	a	b	c	χ^2/ndf
0.50	0.065(62)	0.28(1)	1.0(8)	0.81(46)	0.12
1.00	−0.15(18)	0.07(12)	1.07(7)	0.51(6)	0.68
2.00	0.018(7)	0.44(25)	1.25(8)	0.49(13)	0.64

TABLE VI. RSB fits of zero-temperature data for $[1-q_l]_{\rm av}=a+bL^{-c}$ for different values of the coupling constant ϵ.

ϵ	a	b	c	χ^2/ndf
0.50	0.168(8)	0.73(11)	0.56(7)	0.25
1.00	0.280(8)	1.15(11)	0.57(5)	0.90
2.00	0.378(10)	1.25(6)	0.46(3)	0.45

level. We take Eq. (12) to be our estimate for $d-d_s$. It is consistent with the RSB prediction of zero and also consistent with a small non-zero value in the DP/TNT scenarios.

Data for the average of $1-q_l$ over *all* samples are shown in Fig. 3 along with RSB fits. The data show curvature indicative that corrections to scaling have to be included. The DP/TNT fits, Eq. (6), are shown in Table V, while the RSB fits (which fix μ_l to zero) are shown in Table VI. Both fits have acceptable χ^2.

The cumulative probabilities shown in Fig. 4 give a lot of weight to unphysical negative values of μ_l, especially for $\epsilon=1$. For all values of ϵ the weight is small for μ_l greater than about 0.10 so we conclude that

$$0\leqslant\mu_l\lesssim 0.10. \tag{13}$$

We should, perhaps, be cautious about this statement in view of the large weight at negative values of μ_l in Fig. 4. However, Eq. (13) is consistent with Eq. (12) and the result of Ref. 25 that $\theta'\simeq 0$.

IV. RESULTS AT FINITE TEMPERATURE

In this section we study the model at temperatures well below[25] $T_c\approx 0.63$. Figure 5 shows data for the variance of the link overlap for several low temperatures. The data show strong curvature indicative that a simple fit of the form

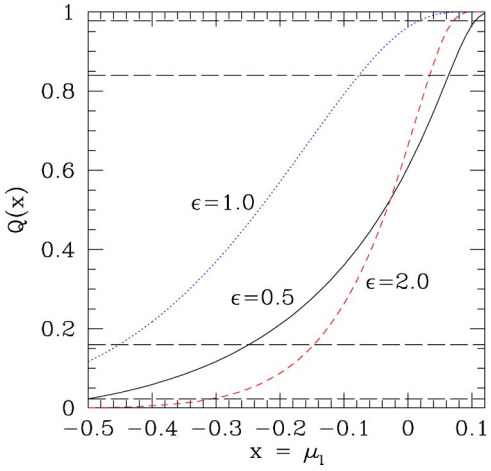

FIG. 4. The cumulative probability for $d-d_s$ from the fits to $[1-q_l]_{\rm av}$ as discussed in the text. The inner pair of dashed horizontal lines show 68% confidence levels and the outer pair show 95.5% confidence levels.

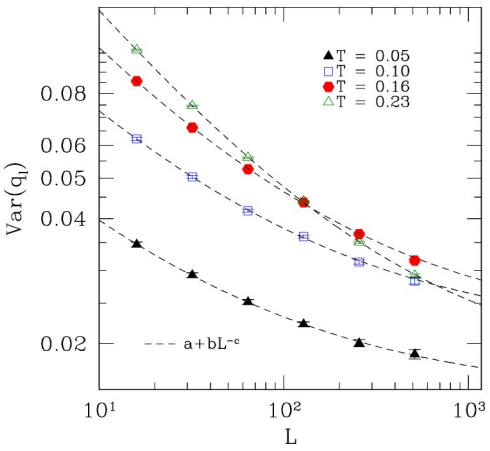

FIG. 5. Log-log plot of finite-T data for the variance of the link overlap $\mathrm{Var}(q_l)$ as a function of system size L for several low temperatures. In all three cases we see strong curvature in the data suggesting corrections to scaling. The dashed lines represent fits according to $a+bL^{-c}$ (RSB) with the fitting parameters shown in Table VIII.

$aL^{-\mu_l}$ is improbable and corrections to scaling must be included.

Fits to Eq. (10) (DP/TNT picture) are shown in Table VII, and fits to the RSB picture (in which μ_l is fixed to be zero) are shown in Table VIII. The quality of the fits is acceptable.

However, the DP/TNT fit for $T=0.05$ gives an unphysical negative value for μ_l with a very small amplitude a. To clarify this situation, we plot, in Fig. 6, χ^2 as a function of μ_l, optimizing with respect to the other parameters (a,b, and c). For $T=0.05$, χ^2 is quite small out to very large *negative* values of μ_l (not shown) and increases rapidly for μ_l greater than about 0.12. Since physically μ_l cannot be negative, the only conclusion we can deduce from the $T=0.05$ data is that μ_l lies between zero and about 0.12, consistent with the result from the $T=0$ data in Eq. (13). The data for χ^2 for $T=0.10$ in Fig. 6 have a minimum at $\mu_l=0.10$ but it is shallow and $\mu_l=0$ has only a slightly greater χ^2 value. The $T=0.10$ data are therefore also consistent with Eq. (13). The data at higher temperatures, $T=0.16$ and 0.23 have a deeper minimum at nonzero χ^2, suggesting that $\mu_l=0$ is somewhat unlikely, but experience from short-range systems[4] suggests that estimates of μ_l at finite T are effective exponents which need to be extrapolated to $T=0$ to get close to the asymptotic value. Hence we do not feel that the results at $T=0.16$ and 0.23 rule out $\mu_l=0$.

Overall, the finite-T data are consistent with μ_l in the range given by Eq. (13) which came from the $T=0$ data, and do not constrain μ_l any further.

TABLE VII. DP/TNT fits of $\mathrm{Var}(q_l)$ to $L^{-\mu_l}(a+bL^{-c})$ for different temperatures.

T	μ_l	a	b	c	χ^2/ndf
0.05	−0.21(54)	0.002(11)	0.073(8)	0.52(35)	0.05
0.10	0.10(11)	0.047(42)	0.16(3)	0.55(24)	0.52
0.16	0.16(6)	0.079(39)	0.29(6)	0.60(17)	0.83
0.23	0.13(8)	0.050(34)	0.41(2)	0.52(2)	1.18

TABLE VIII. RSB fits of $\mathrm{Var}(q_l)$ to $a+bL^{-c}$ for different temperatures.

T	a	b	c	χ^2/ndf
0.05	0.015(2)	0.073(10)	0.47(7)	0.10
0.10	0.020(2)	0.155(11)	0.47(3)	0.47
0.16	0.021(1)	0.261(11)	0.50(2)	1.32
0.23	0.017(1)	0.391(9)	0.55(1)	1.35

V. CONCLUSIONS

We have studied the geometry of the large-scale, low-energy excitations in a one-dimensional Ising spin glass where the interactions fall off as $r^{-\sigma}$ with $\sigma=0.75$, both at $T=0$ and at temperatures well below the spin-glass transition temperature. We find that the fractal dimension of the surface of these excitations, d_s, lies in the range $0\leqslant d-d_s \lesssim 0.05$. This is consistent with the RSB picture ($d-d_s=0$). It is also consistent with the DP/TNT picture ($d-d_s>0$) but with a small value of $d-d_s$. Substantial corrections to scaling had to be incorporated into all the fits.

We have also estimated the exponent $\mu_l=\theta'+2(d-d_s)$, where θ' characterizes the dependence of the energy of droplet excitations on their length scale. We find it to be in the range $0\leqslant\mu_l\lesssim 0.10$, which is consistent with the value for $d-d_s$ in Eq. (12) and our earlier result[25] that $\theta'\simeq 0$. Note that this result for θ', if also valid in the thermodynamic limit, is inconsistent with the DP.

By studying a one-dimensional model, we have been able to study a much larger range of sizes, $16\leqslant L\leqslant 512$, than is generally possible in spin glasses. However, in the absence of a good understanding of corrections to scaling in spin glasses, we still cannot rule out the possibility that different behavior *may* occur in the thermodynamic limit.

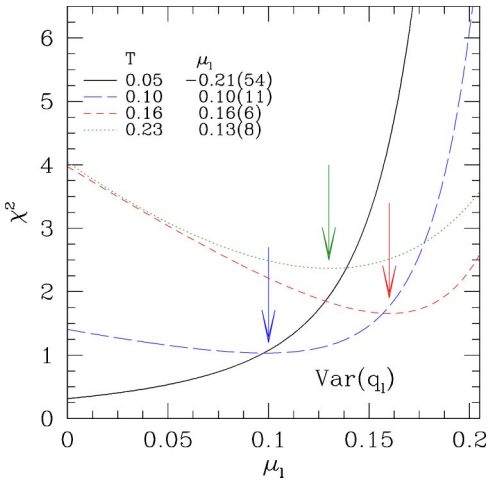

FIG. 6. χ^2 as a function of μ_l, optimized with respect to the other parameters (a,b, and c) in Eq. (10), for the variance of the link overlap. The arrows mark the minima.

ACKNOWLEDGMENTS

We would like to thank K. Tran for carefully reading the manuscript. The simulations were performed on the Asgard cluster at ETH Zürich. We are indebted to M. Troyer and G. Sigut for allowing us to use the idle time on the Asgard cluster. The work of A.P.Y. is supported by the National Science Foundation under Grant No. DMR 0086287.

*Electronic address: peter@bartok.ucsc.edu; URL: http://bartok.ucsc.edu/peter

[1] F. Krzakala and O.C. Martin, Phys. Rev. Lett. **85**, 3013 (2000).
[2] M. Palassini and A.P. Young, Phys. Rev. Lett. **85**, 3017 (2000).
[3] E. Marinari and G. Parisi, Phys. Rev. B **62**, 11677 (2000).
[4] H.G. Katzgraber, M. Palassini, and A.P. Young, Phys. Rev. B **63**, 184422 (2001).
[5] H.G. Katzgraber and A.P. Young, Phys. Rev. B **64**, 104426 (2001).
[6] H.G. Katzgraber and A.P. Young, Phys. Rev. B **65**, 214401 (2002).
[7] J. Houdayer, F. Krzakala, and O.C. Martin, Eur. Phys. J. B **18**, 467 (2000).
[8] J. Houdayer and O.C. Martin, Europhys. Lett. **49**, 794 (2000).
[9] A.J. Bray and M.A. Moore, J. Phys. C **17**, L463 (1984).
[10] W.L. McMillan, Phys. Rev. B **30**, 476 (1984).
[11] W.L. McMillan, Phys. Rev. B **29**, 4026 (1984).
[12] H. Rieger, L. Santen, U. Blasum, M. Diehl, M. Jünger, and G. Rinaldi, J. Phys. A **29**, 3939 (1996).
[13] A.K. Hartmann, Phys. Rev. E **59**, 84 (1999).
[14] M. Palassini and A.P. Young, Phys. Rev. Lett. **83**, 5126 (1999).
[15] A.K. Hartmann and A.P. Young, Phys. Rev. B **64**, 180404 (2001).
[16] A.C. Carter, A.J. Bray, and M.A. Moore, Phys. Rev. Lett. **88**, 077201 (2002).
[17] G. Parisi, Phys. Rev. Lett. **43**, 1754 (1979).
[18] G. Parisi, J. Phys. A **13**, 1101 (1980).
[19] G. Parisi, Phys. Rev. Lett. **50**, 1946 (1983).
[20] M. Mézard, G. Parisi, and M. A. Virasoro, *Spin Glass Theory and Beyond* (World Scientific, Singapore, 1987).
[21] D.S. Fisher and D.A. Huse, Phys. Rev. Lett. **56**, 1601 (1986).
[22] D.S. Fisher and D.A. Huse, J. Phys. A **20**, L1005 (1987).
[23] D.S. Fisher and D.A. Huse, Phys. Rev. B **38**, 386 (1988).
[24] A. J. Bray and M. A. Moore, in *Heidelberg Colloquium on Glassy Dynamics and Optimization*, edited by L. Van Hemmen and I. Morgenstern (Springer, New York, 1986), p. 121.
[25] H.G. Katzgraber and A.P. Young, Phys. Rev. B **67**, 134410 (2003).
[26] A.J. Bray, M.A. Moore, and A.P. Young, Phys. Rev. Lett. **56**, 2641 (1986).
[27] K. Hukushima and K. Nemoto, J. Phys. Soc. Jpn. **65**, 1604 (1996).
[28] E. Marinari, in *Advances in Computer Simulation*, edited by J. Kertész, and I. Kondor (Springer-Verlag, Berlin, 1998), p. 50.
[29] L. Leuzzi, J. Phys. A **32**, 1417 (1999).
[30] M. Palassini, F. Liers, M. Jünger, and A. P. Young, Phys. Rev. B **68**, 064413 (2003).
[31] A.K. Hartmann and A.P. Young, Phys. Rev. B **66**, 094419 (2002).
[32] J.J. Moreno, H.G. Katzgraber, and A.K. Hartmann, Int. J. Mod. Phys. C **14**, 285 (2003).
[33] W. H. Press, S. A. Teukolsky, W. T. Vetterling, and B. P. Flannery, *Numerical Recipes in C* (Cambridge University Press, Cambridge, 1995).